THE LENS AS A NONUNIFORM SPHERICAL SYNCYTIUM

R. T. MATHIAS, J. L. RAE, AND R. S. EISENBERG, *Department of Physiology, Rush Medical College, Chicago, Illinois 60612 U.S.A.*

ABSTRACT The effective intracellular resistivity R_i of the ocular lens is a measure of the coupling between cells. Since degradation of coupling may accompany cataracts, measurements of R_i are of considerable interest. Experimental results show that the lens is a nonuniform syncytium in which R_i is much higher in the nuclear region than in the cortex. A theory describing the lens as a radially nonuniform spherical syncytium is proposed, solved, and described as a simple equivalent circuit. The impedance of the lens is measured with new circuitry which permits the accurate application and measurement of current and voltage over a wide bandwidth without arbitrary compensation of unstable capacitances. The fit of the nonuniform theory to experimental data is satisfactory and the parameters determined are consistent with theoretical assumptions. In the outer region (cortex) of the lens R_i = 3.4 kΩ-cm in the radial direction; in the inner region (nucleus) R_i = 8.3 kΩ-cm, probably as a consequence of differences in coupling and cytoplasmic resistivity. The radial resistivity of the cortex is some five times the circumferential resistivity, demonstrating a marked anisotropy in the preparation, probably reflecting the anisotropy in the orientation of lens fibers and distribution of gap junctions. Current can flow in the circumferential direction without crossing from fiber to fiber; current can flow in the radial direction only by crossing from fiber to fiber.

The electrical properties of most single cells are determined by the properties of the outer membrane and the cytoplasmic solution. Cells of more complex geometry have other structures which contribute to the electrical properties (Eisenberg and Mathias, 1980). For example, most of the sarcolemma of skeletal muscle fibers is invaginated into a T-system. Thus, the electrical properties of skeletal muscle fibers are determined in large measure by the properties of the "inner" membranes (those of the T-system) and the cytoplasm.

Syncytial tissues, consisting of many electrically coupled cells, have still further structural complication. Syncytia have outer membranes in direct contact with the solution surrounding the tissue. Syncytia also have inner membranes, the membranes of the cells which form the tissue, in contact with the extracellular solution within the tissue. The internal resistivity of syncytial tissues is complex since internal current flow is significantly impeded by both the gap junctions between cells and the cytoplasm. Thus, the internal resistivity of syncytial tissues depends on the number and distribution of gap junctions, as well as on the resistivity (ohms-centimeters) of the cytoplasm.

The properties of gap junctions are of interest in many syncytial tissues, since changes in the number, distribution, or properties of junctions would have profound biological implications. It is natural to suspect that many biological processes, as well as experimentally induced perturbations, occur by modification of gap junctions. Measurement of the effective intracel-

lular resistivity, under conditions of constant cytoplasmic resistivity, is one way to determine the overall coupling between cells.

The lens of the eye is a syncytial tissue of approximately spherical geometry. The anterior surface of the lens has a layer of cuboidal epithelial cells covering many layers of lens fibers. These epithelial cells are thought to provide the active transport and metabolism necessary to sustain the fibers which form the bulk of the lens. The lens fibers are coupled together by gap junctions (which presumably also couple epithelial cells to lens fibers) so metabolites and ions, as well as water, can flow from epithelial cell to lens fiber and vice versa. Previous work (e.g., Hogan et al., 1971; Eisenberg and Rae, 1976; Mathias et al., 1979) has shown that the lens can be described as a spherical syncytium consisting of two compartments, an intracellular volume interspersed with a small extracellular space. The extracellular compartment consists of the narrow spaces between cells. The intracellular compartment consists of the cytoplasm of the lens fibers and the gap junctions coupling cells. The effective intracellular resistivity of the lens thus depends on the coupling between cells. The amount of coupling between cells is particularly important in the lens, because inner fiber cells have little or no ability to extrude sodium (evidence reviewed in Rae, 1979). Thus, uncoupling of cells would necessarily lead to swelling and eventual rupture of the lens fibers and could contribute to cataractogenesis (Tanaka et al., 1980).

The measurements presented here are made with new circuitry that has some general interest and so is described in detail. The fundamental requirements of measurement with microelectrodes are the faithful recording of potential over a wide bandwidth, the application of a controlled amount of current, and the measurement of that current. A simple circuit is presented here which permits the accurate recording of potential and measurement of current over a bandwidth of more than 10 kHz without compensation of stray capacitance. Another circuit is presented which applies current, independent of the resistance of the microelectrode, and simultaneously measures the potential on top of the current microelectrode, both over a wide bandwidth. Neither of these circuits seems widely used and, in our opinion, each offers significant advantages in performance, simplicity, and cost over those in common use.

For example, many workers (see reference list in Suzuki et al., 1978) use "negative capacity" circuits to record membrane potential with microelectrodes. Such circuits try to compensate the capacitance between the top of the voltage microelectrode and ground by injecting an equal and opposite current derived from the output of the voltage recording amplifier. A negative capacity circuit useful for quantitative experiments must meet several problems: (*a*) The production of a negative capacity current, precisely equal and opposite to the actual capacity current, at frequencies to 10 kHz is not trivial and the accuracy of the negative capacity currents must be demonstrated by direct measurement. (*b*) The adjustment of the amount of negative capacitance must be objective, independent of the resistance of the microelectrode or properties of the amplifiers, and accurate. For impedance measurements, adjustment must be made while the operation of the circuit is observed in the frequency domain, preferably by phase measurements. (*c*) The stray capacitance being compensated must be stable during an experiment; it should not depend on the level of solution, or the location of nearby conducting objects (like the experimenter). (*d*) The negative capacitance circuit should not introduce excess noise. Since negative capacity circuits rarely, if ever, satisfy the criteria just mentioned, the circuits proposed here may have some attractions.

The theory previously used to interpret electrical measurements from the lens represented it as a spherical syncytium with uniform properties (Eisenberg et al., 1979; Mathias et al., 1979). Measurements interpreted with this theory led to results inconsistent with its assumptions; namely, the effective intracellular resistivity R_i was found to vary systematically with location (see Results). A new theory was therefore needed to describe the nonuniform properties of the lens. This theory is derived in the Appendix and described in the Theory section.

Our main conclusion is that the lens must be described as a nonuniform syncytium consisting of a spherical inner region (the nucleus) and an outer cortical region. The effective intracellular resistivity of the nucleus is some 2.4 times larger than that of the cortical region. The resistivity to radial current flow in the cortical region is five times larger than the resistivity to circumferential current flow. These electrical properties probably reflect the distribution of gap junctions and the variation of cytoplasmic resistivity. The effect of various interventions thought to uncouple cells can be determined by the methods presented here.

THEORY

Nonuniform Theory: Impedance of a Composite Lens

We describe the lens as a composite spherical syncytium, surrounded by an outer membrane with specific admittance $Y_s = G_s + j\omega C_s$ (Siemens per square centimeter). (The symbols used in this paper closely conform with the symbols defined in Eisenberg et al., 1979. See the Glossary of that paper for definitions.) The inner and outer regions of the lens consist of two interspersed compartments, an extracellular compartment of effective resistivity R_e accessible by diffusion from the outside bathing solution, and an intracellular compartment consisting of the solution within cells and the gap junctions between cells. The membrane separating the intra- and extracellular space is described by an admittance $Y_m = G_m + j\omega C_m$.

The analysis presented is a generalization of the theory of Eisenberg et al., 1979. We include two regions of the spherical syncytium, one extending from the center to the radial location $r = b$ with effective intracellular resistivity αR_i, and the other extending from the radial location $r = b$ to the outer edge of the lens ($r = a$) with effective intracellular resistivity R_i. We do not allow each of the electrical and structural characteristics of the lens to differ in the two regions because the available data do not justify, let alone require, the resulting increase in complexity of the notation and algebra. Inclusion of different characteristics in the two regions is straightforward, nonetheless, and can be done by simple repetition of the steps presented in the Appendix, if necessary.

If current i_L is applied in the center of the lens, the equation for the intracellular potential in the inner region is

$$\left.\begin{aligned} &(1/R_i)\nabla^2 U_i - \alpha Y_m (S_m/V_T)(U_i - U_e) = -\alpha i_L \delta(\vec{r}) \\ &\text{The equation for the extracellular medium is} \\ &(1/R_e)\nabla^2 U_e + Y_m (S_m/V_T)(U_i - U_e) = 0 \end{aligned}\right\} 0 \le r \le b. \qquad (1)$$

The partial differential equation for current flow in the intracellular medium in the outer region is

$$\left.\begin{aligned}&(1/R_i)\nabla^2 U_i - Y_m(S_m/V_T)(U_i - U_e) = 0\\ &\text{and for the extracellular medium}\\ &(1/R_e)\nabla^2 U_e + Y_m(S_m/V_T)(U_i - U_e) = 0\end{aligned}\right\} b \le r \le a. \tag{2}$$

The boundary between the two regions is characterized as the contact between two resistive media. There is continuity of current and continuity of potential across the boundary within both the intra- and extracellular medium. In the following equations the superscript "+" indicates a variable evaluated just outside the sphere $r = b$ and the superscript "-" indicates a variable evaluated just inside that sphere. The intracellular medium at $r = b$ is described by

$$U_i(b^+) = U_i(b^-)\,. \tag{3}$$

If the the flow of intracellular current is continuous across the boundary $r = b$, but the effective intracellular resistance changes, then there will be a proportional change in the spatial derivative of the intracellular voltage.

$$\frac{\partial U_i(b^-)}{\partial r} = \alpha \frac{\partial U_i(b^+)}{\partial r}\,. \tag{4}$$

The extracellular medium at $r = b$ is described by

$$U_e(b^-) = U_e(b^+) \tag{5}$$

$$\frac{\partial U_e(b^-)}{\partial r} = \frac{\partial U_e(b^+)}{\partial r}\,. \tag{6}$$

The following equations describe the outer boundary of the lens. The first two equations are boundary conditions. The third is an integral constraint which is a direct consequence of conservation of current or can be derived from the differential equations, the divergence theorem, and the boundary condition (see Eisenberg et al., 1979, p.169)

$$U_e(a) = 0 \tag{7}$$

$$\frac{\partial U_i(a)}{\partial r} = -R_i Y_s U_i(a) \tag{8}$$

$$\frac{1}{R_i}\int_{r=a} \frac{\partial U_i(a)}{\partial r}\,dS + \frac{1}{R_e}\int_{r=a} \frac{\partial U_e(a)}{\partial r}\,dS = -i_L. \tag{9}$$

Eqs. 1–9 specify the nonuniform theory. The physical and physiological interpretation of these equations is presented in more detail in Eisenberg et al., 1979.

The Appendix to this paper presents an outline of the solution of the equations using the techniques of perturbation theory. The results of that analysis are expressions for the dominant term in the extracellular potential

$$U_e^{(0)}(r) = \frac{i_L}{4\pi a^2(Y_s + Y_e)}\left[1 - \frac{a}{r}\frac{\sinh \gamma r}{\sinh \gamma a}\right], \tag{10}$$

where the symbols are defined in Fig. 1.

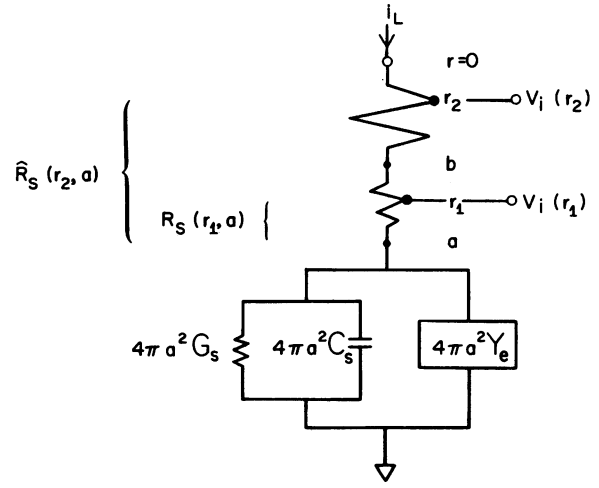

FIGURE 1 The equivalent circuit of a nonuniform syncytium. The lens is described here as a spherical syncytium consisting of a nucleus with one effective intracellular resistivity surrounded by a cortex with another resistivity. The dominant terms of the solution of the syncytial partial differential equations describe the equivalent circuit shown. Each component of the circuit has a simple physical meaning. The terminal at the top of the figure represents the center of the lens, where current is injected. The tapered resistor represents the local potential produced by the point source. The amount of series resistance $R_s(r,a)$ observed depends on the location of the electrode and the radius of the lens, as well as on the effective intracellular resistivity of the syncytium between the location r and the outer membrane. The capacitance and resistance shown represent the properties of a hypothetical outer membrane of the lens. They probably correspond to an average of the properties of the anterior epithelia and to the outermost layer of both anterior and posterior lens fibers. The admittance Y_e describes the inner membranes: $Y_e = (\gamma/R_i + R_e)\{\coth\gamma a - 1/\gamma a\}$, where $\gamma = [(R_i + R_e)(S_m/V_T)(G_m + j\omega C_m)]^{1/2}$. The $O(\epsilon)$ correction terms are given in the text.

Two expressions are required to describe the intracellular potential. One expression is for the outer region defined by $b \leq r_1 \leq a$

$$U_i(r_1) = i_L\left[\frac{1}{4\pi a^2(Y_s + Y_e)} + \frac{R_i}{4\pi}\left(\frac{1}{r_1} - \frac{1}{a}\right)\right] + O^+(\epsilon). \tag{11}$$

The other expression is for the region defined by $0 \leq r_2 \leq b$

$$U_i(r_2) = i_L\left[\frac{1}{4\pi a^2(Y_s + Y_e)} + \frac{R_i}{4\pi}\left(\frac{1}{b} - \frac{1}{a}\right) + \frac{\alpha R_i}{4\pi} + \left(\frac{1}{r_2} - \frac{1}{b}\right)\right] + O^-(\epsilon). \tag{12}$$

The symbols $0^+(\epsilon)$ and $0^-(\epsilon)$ describe the correction terms (Eqs. 13–16) for the outer and inner regions, respectively. The correction terms contain only ϵ, ϵ^2, and higher order terms. Thus, the correction terms will be unimportant as long as ϵ is much smaller than 1, unless the numerical value of other factors is large enough to offset the small value of ϵ. In our problem the other factors are large only near the point source. Thus, we can expect Eqs. 11 and 12, and the equivalent circuit they represent (Fig. 1), to be reasonably accurate away from the point source, when $\epsilon << 1$.

The tapered resistor in Fig. 1 represents the local potential produced by the point source located in the center of the preparation. This potential would be everywhere described by the simple expression in Eq. 11 if the preparation had uniform properties. When the preparation

has nonuniform properties, the resistance requires a more complicated description. The series resistance between two locations x_1 and x_2 is described by the function $R_s(x_1,x_2)$. The resistance from the boundary between inner and outer regions and the outer edge of the preparation is thus $R_s(b,a) = (R_i/4\pi)[1/b) - (1/a)]$. The resistance between a voltage electrode located in the outer region at $r = r_1$ and the outer membrane is $R_s(r_1,a) = (R_i/4\pi)[1/r_1) - (1/a)]$. The resistance between an electrode in the inner region located at $r = r_2$ and the outer membrane is slightly more complicated because of the different resistivities of the two regions. The total series resistance $\hat{R}_s(r_2,a)$ is then the composite of a series resistance in each region, namely $\hat{R}_s(r_2,a) = R_s(b,a) + R_s(r_2,b)$, where $R_s(r_2,b) = (\alpha R_i/4\pi)[1/r_2) - (1/b)]$.

The equivalent circuit shown in Fig. 1 is useful in predicting and explaining the qualitative properties of the nonuniform model. It is clear, for example, that measurements in the outer region are insensitive to the intracellular resistivity of the inner region. The series resistance caused between the tip of the current microelectrode and the voltage electrode simply changes the effective resistance of the current electrode. The intracellular resistivity of the inner region thus has only second order effects on the potential $U_i(r_1,j\omega)$.

The expressions 11 and 12 leave out higher order terms which, on occasion, contribute a small but noticeable amount to the impedance at certain frequencies. These terms are

$$O^+(\epsilon) = -\epsilon[U_e^{(0)}(r_1) + U_e^{(0)}(0)] - \epsilon(1-\alpha)\left[\frac{i_L}{4\pi a^2(Y_s + Y_e)} - U_e^{(0)}(0)\right]\mathbf{C} + \epsilon^2(\ldots) \quad (13)$$

$$O^-(\epsilon) = -\epsilon\alpha[U_e^{(0)}(r_2) + U_e^{(0)}(0)] - \epsilon(1-\alpha)\left\{\left[\mathbf{C}\left(\frac{i_L}{4\pi a^2(Y_s + Y_e)}\right) - U_e^{(0)}(0)\right] - U_e^{(0)}(\mathrm{b})\right\} + \epsilon^2(\ldots) \quad (14)$$

where

$$\mathbf{C} = 1 - \frac{\mathbf{G}'(\gamma b) + \mathbf{C}_0 \frac{a \sinh \gamma b}{b \sinh \gamma a}\left[\left(1 + \frac{\gamma b \coth \gamma b}{2}\right)\left(\coth \gamma b - \frac{1}{\gamma b}\right) - \frac{\gamma b}{2}\right]}{\mathbf{W}'(\gamma b) - \mathbf{W}(\gamma b)\left[\coth \gamma b - \frac{1}{\gamma b}\right]}, \quad (15)$$

where prime indicates differentiation with respect to the normalized radial coordinate r; the above expressions are evaluated at $r = \gamma b$; and the functions $G(r)$, $W(r)$, and C_O are defined in the Appendix. Note that the expressions given reduce to the result obtained by Eisenberg et al., 1979, when $\alpha = 1$. The form of the expressions are slightly different, however.

Eqs. 10–15 define the nonuniform model. The entire model, including the correction terms 13 and 14, was fit to the experimental data, using $b = 0.65a$. The reduced model, shown in Fig. 1, is quite helpful qualitatively, but was never used quantitatively. Curve fitting of the data was done with the complete solution up to $O(\epsilon^2)$, as defined by Eqs. 10–15.

METHODS

Voltage Recording

The accuracy of the circuits shown in Fig. 2 is limited by the stray capacitances shown in Fig. 3. There are three sources of stray capacitance: the microelectrodes, the input of the operational amplifiers, and the shielded wires connecting devices.

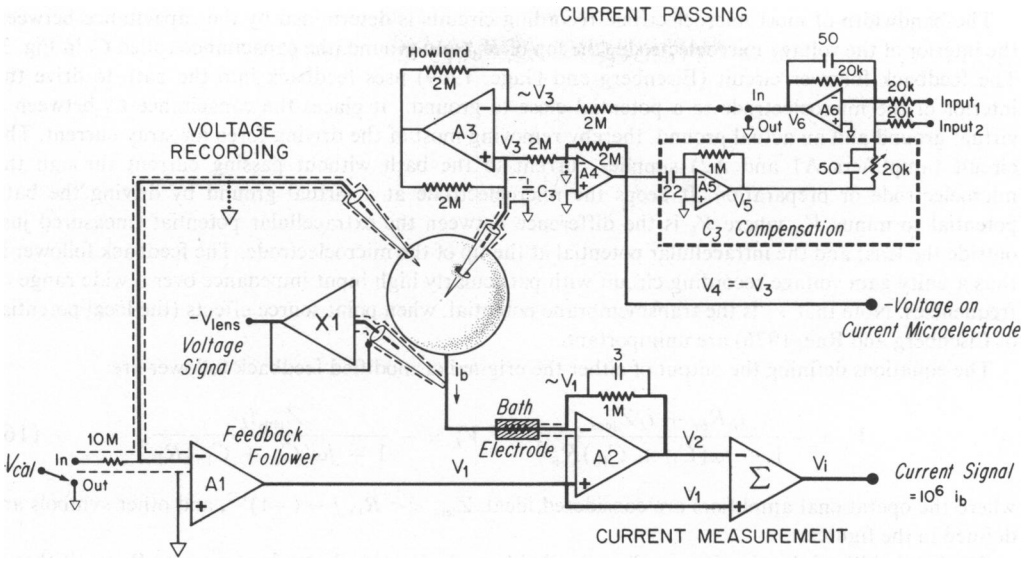

FIGURE 2 A description of the electronics and preparation. The main signal paths are shown as heavy lines. Shielding is shown as a dashed line. Virtual grounds are shown as dotted lines to common. The dashed square shows the stray capacitance C_3; the other capacitances are circuit components. Capacitances are given in picofarads and resistances in ohms. The amplifier marked × 1 is a unity gain buffer; the amplifier marked Σ is an operational amplifier connected as a unity gain summer. The voltage recording circuit is a feedback follower which drives the tip of the voltage microelectrode to a virtual ground and the bath to minus the "membrane" potential. The amplifiers A2 and Σ allow current measurement. The voltage signal used for analysis is V_{lens}, since that signal is independent of potential drops in the bath or bath electrodes. The current passing circuit is a modification of the Howland circuit which allows direct measurement of the potential on the top of the voltage electrode. A compensation circuit is used to improve the speed of the Howland; imperfections in compensation do not affect the measured potential or current.

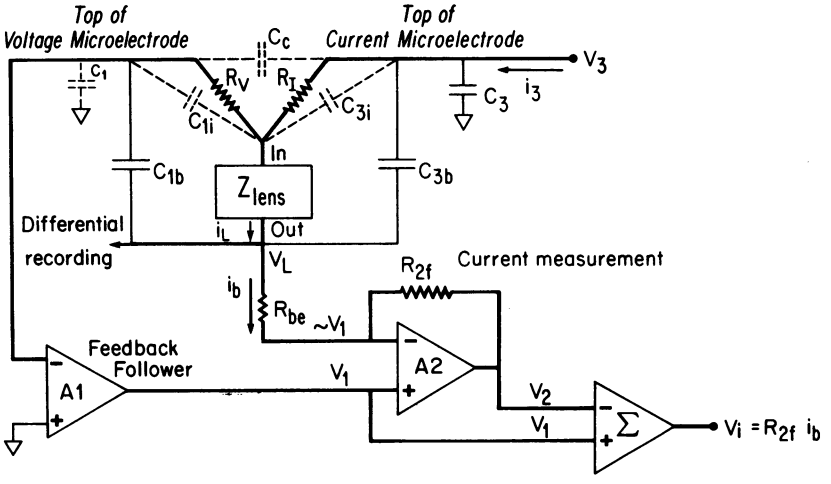

FIGURE 3 The stray capacitances in the set-up. All of the capacitances shown in this figure are stray capacitances; none are circuit elements. The dashed capacitances are negligible with the precautions described in the text. The main signal paths are shown as heavy lines.

The bandwidth of most microelectrode recording circuits is determined by the capacitance between the interior of the voltage microelectrode (the top of R_V) and ground, the capacitance called C_1 in Fig. 3. The feedback follower circuit (Eisenberg and Gage, 1969) uses feedback into the bath to drive the interior of the microelectrode to a potential close to ground: it places the capacitance C_1 between a virtual ground and an actual ground, thereby removing most of the driving force for stray current. The circuit (amplifiers A1 and A2) supplies current to the bath without passing current through the microelectrode or preparation. It keeps the microelectrode at a virtual ground by driving the bath potential to minus V_L, where V_L is the difference between the extracellular potential (measured just outside the lens) and the intracellular potential at the tip of the microelectrode. The feedback follower is thus a unity gain voltage recording circuit with particularly high input impedance over a wide range of frequencies. Note that V_L is the transmembrane potential, when point source effects (the local potential of Eisenberg and Rae, 1976) are unimportant.

The equations defining the output of either the original or modified feedback follower are:

$$V_1 \simeq -\frac{i_b R_{be} + i_L Z_{\text{lens}}}{1 + j\omega(C_{1i} + C_{1b})R_V}; \qquad V_L \simeq -\frac{Z_{\text{lens}} i_L}{1 + j\omega(C_{1i} + C_{1b})R_V}, \tag{16}$$

where the operational amplifiers are considered ideal, $Z_{\text{lens}} << R_V$, $j = (-1)^{1/2}$, and other symbols are defined in the figures.

The bandwidth of the circuits may be extended by reducing the electrode resistance R_V, or, if that is impractical, by reducing the stray capacitance C_{1b} with shielding described later. The residual delay introduced by the feedback follower and associated stray capacitances can be measured and then analytically removed by measuring the response to the calibration input V_{cal}.

$$V_L \simeq -\frac{10^{-7} R_V}{1 + j\omega(C_{1i} + C_{1b})R_V} V_{\text{cal}}. \tag{17}$$

Note that the feedback follower can be used, with the switch "In," to apply current ($= V_{\text{cal}}/10^7$) to the preparation, independent of the electrode resistance or lens impedance.

Eq. 17 assumes that the 10-MΩ calibration resistor is a pure resistor without stray capacitance. If the resistor is embedded in a grounded shielded cable and wired directly to the inverting input of the operational amplifier, the stray capacitances around the resistor can be made sufficiently small to allow calibration up to frequencies of 10 kHz. (The properties of the calibrating impedance can be directly measured by replacing R_V with a low value resistor, say 100 kΩs.) In wide-band applications one might replace the calibration resistor with a small capacitor.

The switching arrangements on the calibration input indicated in Fig. 2 are necessary to reduce pick-up in the 10-MΩ resistor while keeping stray capacitance to a minimum. For the same reasons, the lead from the resistor to the switch must be enclosed in a shielded and grounded cable. All the metal around the switch should also be grounded.

The circuit used here is more complex but more useful than earlier feedback followers (Eisenberg and Gage, 1969; Mathias et al., 1979) because it allows measurement of the current flowing through the preparation. In the present circuit, the output of amplifier A1 is connected to the noninverting input of operational amplifier A2, which itself is wired as a current-to-voltage converter. The potential at the inverting input of A2 is virtually the same potential as the output of amplifier A1. Amplifiers A1 and A2 act together to control the bath potential (and the potential inside the voltage microelectrode) just as in simpler feedback follower circuits, where the output of amplifier A1 is directly connected to the bath.

The feedback follower circuit illustrated in Figs. 2 and 3 is expected to have wide bandwidth, because of the reduced potential across C_1.[1] The bandwidth of the feedback follower is determined to a first order by the resistance of the voltage electrode and the capacitance between the interior of the microelectrode and the bathing solution, shown as C_{1b}, typically a few picofarads for each millimeter the microelectrode

[1]Because C_1 has important second order effects, it should be kept small by connecting the inverting input of amplifier A1 to the voltage microelectrode with a short length of low capacitance cable.

is immersed in the bathing solution. If very wide bandwidth is needed, the voltage microelectrode should be shielded with conductive paint (Valdiosera et al., 1974) connected to ground and insulated from the bath with varnish (Fig. 3). Then, capacitances of $C_{1b} = 0.2$ pF can be easily obtained. Too small a value of the time constant R_1C_{1b} will underdamp the system, inducing noise or instability[2] and so should be avoided.

In the present experiments noise was minimized at the expense of bandwidth by leaving the voltage electrode unpainted: a bandwidth of a few kilohertz is more than adequate to specify the relevant electrical properties of the lens (Mathias et al., 1979).

The output V_1 of the feedback follower (amplifier A1) measures the sum of the lens potential, the potential drop in the bath, and the potential drop across the bath electrode (Eq. 16). On the other hand, the potential V_L just outside the preparation is independent of the uninteresting potential drops within the bath or across the bath electrodes. Bath potentials are particularly troublesome in preparations such as the lens with small total (i.e., input) resistance. For that reason, we record the potential V_L instead of V_1. Measurement of V_L is equivalent to a differential recording of "membrane" potential in more conventional circuits, but here problems of common mode rejection are minimal. V_L is measured with a differential "micro"-electrode of low resistance (500 kΩs) connected to an operational amplifier in unity gain configuration. This extracellular microelectrode is made from a standard micropipette with a broken tip, filled with a 3-M KCl-1% agar solution. Bandwidth is extended by using an amplifier with reasonably low input capacitance and surrounding the differential electrode with a driven shield. The small residual phase shifts were measured in each experiment and removed in subsequent data processing.

Current Measurement

The feedback follower circuit presented here includes extra amplifiers to allow the measurement of current. Amplifier A2 measures the current I_b flowing through the bath electrode resistance R_{be}. The output of A2 is (at DC) $V_2 = -i_bR_{2f} + V_1$. Subtraction of V_2 from V_1, in the differential amplifier shown (Fig. 2), gives a current signal $V_i = R_{2f}i_b$.

The largest error in the measurement of current is not produced by the current measuring circuit, but by current flow into the bath through the capacitance C_{3b} of the glass wall of the current microelectrode. This capacitive current ensures that i_b, the current measured, does not equal i_L, the current into the preparation. Rather, $i_b \simeq i_L + j\omega C_{3b}V_3$. The capacitive current flow through C_{3b} can also produce significant potentials within the bath (Valdiosera et al., 1974). The capacitance is therefore minimized by painting the current microelectrode; the differential recording of V_L already described removes the effect of bath potentials.

Other stray capacitances are significant in wide-band operation. Shielding of at least one of the electrodes is always necessary to make the coupling capacitance C_c negligible. Wide-band recording (> 5 kHz) requires shielding of both microelectrodes. The capacitance C_3 (from the current microelectrode to ground) has no effect on the measured potential or measured current. It does affect the relationship between current generated by a constant current circuit i_3 and the current flowing through the preparation i_L and is discussed later in that context.

When recording from the lens, the voltage microelectrode is often placed hundreds of micrometers into the preparation. The current microelectrode is usually at the center of the lens (to ensure symmetry in the extracellular potential), also some hundreds of micrometers from the surface. The capacitances C_{1i} and C_{3i} cannot be shielded without certain damage to the lens. We therefore use low resistance electrodes to minimize capacitive coupling into the lens interior. Fortunately, the lens tolerates insertion of electrodes with 1–3 MΩ resistance with the loss of only a millivolt or two of resting potential.

Current Passing Circuitry

The circuitry already described would suffice for many purposes since it allows the recording of potential and measurement of current. The current might be applied to the microelectrode and preparation simply

[2]Levis, R. Personal communication.

by driving V_3 from the output of a voltage generator.[3] This arrangement, however, will often not allow application of a controlled amount of current to the preparation because the microelectrode resistance is a notoriously variable property. For the current to be constant, it must be independent of the resistance of the current microelectrode.

The Howland circuit (Smith, 1971; Eisenberg and Gage, 1969) provides good control of the current i_3 (Fig. 3) within the output limitations of the amplifier A3 and the bandwidth limitations about to be discussed. The conventional Howland circuit does not, however, allow the measurement of the potential V_3 on the top of the microelectrode, because connection of even a high input impedance device to the inverting input of amplifier A3 would seriously degrade the performance of the circuit. (It would significantly increase the capacitance C_3 and thus slow the circuit as discussed later in this section.) The measurement of V_3 is desirable because it allows measurement of the electrode resistance, the resting potential, and the impedance of the preparation. The resting potential is measured by V_3, if there is no current applied from the Howland (i.e., if the switch in the output of amplifier A6 is "Out," Fig. 2). Then, the change in V_3 when the current microelectrode penetrates the lens is a measure of resting potential and of the success of the penetration. When the switch is "In," the measured value of V_3 can be used directly to measure the phase angle of the impedance of the preparation, if the current i_L through the preparation is in phase with the potential V_3 (Falk and Fatt, 1964; Valdiosera et al., 1974.

The amplifier A4 is included in our modified Howland circuit to allow measurement of V_3. Amplifier A4 is wired as a unity gain inverter, so its output $V_4 = -V_3$. The inverting input of amplifier A4 is at virtual ground and the operation of the Howland circuit is hardly changed: amplifier A3 and its associated circuitry still control the current i_3 to a value independent of the electrode resistance R_l.

Unfortunately, the control of the total current i_3 does not ensure the control of the current i_L flowing into the preparation. The total current supplied by the Howland circuit divides into three components, only one of which (i_L) flows into the preparation. Another component flows directly into the bath through C_{3b}. In the case of the lens, this second component of current (through C_{3b}) is small, because the electrode is shielded to within 100–200 μm of its point of insertion into the lens. The third component of current flows through the capacitance C_3 to ground[4] and presents a more substantial problem. This current is irrelevant to the lens, since it bypasses the preparation entirely. Yet, the amplifier A3 supplies and controls the irrelevant, as well as relevant, component. For example, if a rectangular pulse of current is demanded from the Howland circuit, the voltage V_3 will follow a charging curve, a saturating exponential with time constant R_lC_3 (if the electrode resistance is constant). Thus, the current through the preparation will not be rectangular, but will also follow a saturating exponential (since $i_L \simeq V_3/R_l$). Only the sum i_3 of the irrelevant capacity current and the current through the preparation will be rectangular.

Circuitry has been developed to compensate for the current through C_3, thus allowing the Howland circuit to control the current into the preparation i_L. If the compensation were perfect, the current $i_b \simeq i_L$ would be determined by input_1 plus input_2. It should be clearly realized that the compensation scheme is included only to allow the delivery of constant current to the preparation. The measurement of the potentials V_{lens}, V_3, or of the current i_L, flowing through the preparation, is unaffected by the compensation scheme. Thus, the errors inevitably present in any compensation scheme will not bias our results.

The compensation circuit (amplifier A5 and associated components) differentiates the voltage V_3 on top of the current microelectrode and adds an adjustable amount of that differentiated signal into the input (V_6) controlling the current applied. Since the irrelevant current through C_3 is proportional to the derivative of V_3, this feedback scheme acts to remove the effect of C_3. The amount of compensation, described by $O \leq \chi \leq 1$, is adjusted by the 20k potentiometer to provide an optimal response judged by

---

[3]The voltage generator is best connected through a large series capacitor to avoid a shunt from the cell interior to ground which eventually has harmful effects on small preparations. An electrolytic capacitor should not be used, because it is likely to have significant leakage current.

[4]The capacitance C_3 is formed by the input capacitance of amplifier A4, the capacitance of the cable to the microelectrode, and the capacitance from the microelectrode interior to the shielding paint.

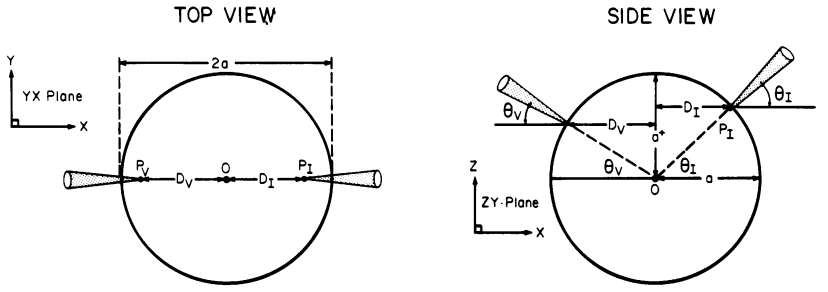

FIGURE 4 The placement of microelectrodes. The lens and microelectrodes are shown in top and side views. The point of penetration of the voltage and current electrodes are called P_V and P_I, respectively. The angles of penetration are called θ_V and θ_I. The center of the lens is called O = (0,0,0), and the plane of each view is indicated by the coordinates. The electrodes are held at the angle shown. They are placed over the points of penetration by their micromanipulators and then advanced along the penetration track, from $P_{V,I}$ to the center of the lens O, by piezoelectric electrode positioners which allow large (centimeters), but precise (±0.02 μm), excursions (centimeters) in one direction.

the current signal V_i or the voltage signal V_3. The criteria for optimal response will depend on the measurement being made.

The current passing circuit is described by the following equations:

$$\begin{array}{ll} \text{Uncompensated} & \text{Compensated} \\ i_L = -\dfrac{V_{\text{input}}}{2 \times 10^7} - C_{3b}\dfrac{dV_3}{dt} & i_L = -\dfrac{V_{\text{input}}}{2 \times 10^7} - \chi C_{3b}\dfrac{dV_3}{dt}, \end{array} \tag{18}$$

where $V_{\text{input}} = \text{input}_1 + \text{input}_2$.

Implementation of Circuits

The circuits shown were implemented with the operational amplifier model 48K of Analog Devices, Inc., Norwood, Mass. If long lengths of shielded cable need to be driven, line drivers[5] should be incorporated into the circuit to drive the cable capacitance. If the output of the circuits is connected to devices with independent power supplies (e.g., oscilloscopes, Fourier analyzers, or A/D converters), it may be necessary to place a differential buffer stage (i.e., a wide-band instrumentation amplifier) after the cable and before the analyzer or converter. The inverting input of the buffer stage should be connected to the ground of the output circuit (e.g., of the line driver).

Circuits used to switch inputs and outputs and provide gain are not shown. These are straightforward, but require some care in design and wiring to avoid crosstalk, noise, or restricted bandwidth.

Experimental Procedure

The lens of a frog eye was dissected and transferred to the Ringer's solution described in Mathias et al., 1979. The chamber used allowed continuous exchange of the bathing solution.

We wished to place the current microelectrode as near as possible to the center of the lens. Fig. 4 presents a side and top view of the lens. The top view corresponds to the image seen in the compound microscope. The microelectrodes were held parallel at fixed known angles of penetration θ_V and θ_I by the rigidly constructed electrode holders. The diameter $2a$ and center O = (0,0,0) of the lens were determined in a filar eyepiece. The distances D_V and D_I were calculated by $D_{V,I} = a \cos \theta_{V,I}$ and were marked off from the center of the lens by the filar eyepiece to determine the points of penetration P_V and

[5]A line driver can be a unity gain configuration of an operational amplifier insensitive to capacitive load and with large output current capability.

P_I. The electrodes were placed at P_V and P_I by micromanipulation in the XYZ planes. The current electrode was advanced along the dotted line a distance a^+ (shown in the side view) by an electrode positioner which measures the distance advanced (Inchworm, model PZ-555, Burleigh Instruments, Fishers, N.Y.). The distance a^+ was taken as $0.95a$ because the lens is an oblate spheroid (i.e., has the shape of a hamburger bun) with its shortest axis along the Z coordinate. The positioning of the electrode could be independently confirmed by microscopic observation. When the light intensity was reduced in the compound microscope, the biological center of the lens could be visualized as a whirl. The electrode location determined geometrically was typically within 50 μm of the biological center. Finally, the voltage electrode was inserted and advanced by a second electrode positioner. Measurements were made at various penetrations along the inward track, shown as a dotted line in the side view. Again, the position of the electrode was confirmed by microscopic observation.

Data Analysis

A stochastic current was applied to the lens and the resulting induced voltage was analyzed according to the general procedures described in Mathias et al. (1979). The method of analysis described in that paper was improved in several ways. Fourier analysis of 256 frequency points was performed on a Fourier analyzer (model 5420; Hewlett Packard Co., Palo Alto, Calif.) which implements overlap processing and a combination of analog and digital anti-aliasing filters. These features, combined with the improved circuitry already described, substantially decreased the variance of measurements. Thus, the time required to acquire impedance data was greatly reduced and no data smoothing was needed. Wild-point editing was performed; wild points were almost always confined to multiples of the line frequency. Three data sets, each a subset of the total frequency range 0.08–800 Hz, were usually recorded at each of four radial locations. The three data sets provide a total of 768 frequency points at each location. The three data sets were merged into a single data set consisting of the magnitude and phase angle at 200 frequencies.[6] The frequencies were selected to provide approximately equal spacing on a logarithmic frequency scale. Curve fitting was performed on the unsmoothed magnitude and phase data taken at one radial location or on a composite of the data taken at several radial locations. In the latter case, 50 pairs of data were selected at each radial location and combined into a composite data set, spanning the properties at all four radial locations. The 50 pairs of data were chosen to provide approximately equal spacing on a logarithmic frequency scale across the whole frequency range. Curve fitting to the composite data set determined the 7 parameters of the theory described in the Appendix (Table II). The significance and independence of the estimates of parameters were tested as described in Mathias et al. (1979).

RESULTS

Exploratory experiments were made to test the theory of Eisenberg et al. (1979) using impedance data recorded with the circuits and procedures of Mathias et al. (1979) at two locations within the lens. That theory idealizes the lens as a a radially uniform (although perhaps anisotropic) tissue with a simple membrane boundary condition. The results of this preliminary analysis are shown in Table I.

The value of the effective intracellular resistivity R_i, determined with the uniform model, clearly depends on the location at which it is measured. The other parameters which could be determined in these exploratory experiments were the specific surface conductance G_s in Siemens per square centimeter; the inner capacitance C_m in microfarads per square centimet-

[6]The data taken at the other 568 frequencies were not used. The raw data at 200 points were sufficiently smooth and dense to provide excellent estimates of impedance, without use of the smoothing procedure of Mathias et al. (1979). A much larger and faster computer would be needed to curve fit to all the data acquired.

TABLE I

CIRCUIT PARAMETERS MEASURED AT TWO LOCATIONS USING THE UNIFORM MODEL AND PRELIMINARY DATA

Lens	r/a	G_s	C_m	R_i	R_e	C_s	G_m
		($\mu S/cm^2$)	($\mu F/cm^2$)	($k\Omega$-cm)	($k\Omega$-cm)	($\mu F/cm^2$)	($\mu S/cm^2$)
1–1	0.79	83	1.70	3.8	90	3.2	1.34
	0.37	72	1.70	7.5	138	*	1.56
1–2	0.80	192	0.76	2.5	49	2.7	0.48
	0.34	190	0.65	6.2	67	*	0.47
1–3	0.78	64	1.25	2.8	81	2.9	*
	0.35	83	0.91	5.5	82	*	1.37
1–4	0.79	300	0.69	3.7	44	8.4	0.44
1–5	0.79	213	0.91	2.8	53	5.7	*
	0.37	303	0.58	5.4	54	*	0.88
1–6	0.79	395	0.67	2.8	49	8.4	*
	0.37	292	0.78	3.1	45	*	0.049
1–7	0.80	144	0.61	3.0	88	4.0	*
	0.39	181	0.81	4.6	106	*	0.53
1–8	0.79	139	0.88	4.3	71	9.5	*
	0.38	181	0.86	5.9	64	*	0.65
1–9	0.80	96	1.24	2.9	92	4.4	*
	0.35	81	0.89	3.7	70	*	1.2
				Summary			
Outer location							
Mean	0.79	173	1.00	3.11	72	5.47	0.77
SEM	0.01	32	0.13	0.22	7	0.94	0.16
Inner location							
Mean	0.39	166	0.90	5.24	78		
SEM	0.01	37	0.12	0.50	11		
Outer/inner							
Mean	1.04	1.10	1.68	0.92			
SEM	0.29	0.19	0.12	0.17			

The lenses chosen had a radius of 1.2 mm.

*The value was not determined independently; rather, it was constrained to the value measured at the other location.

er; and the effective extracellular resistivity R_e in kilohm-centimeters. None of these variables show significant variation with position of measurement. In most experiments the specific capacitance C_s of the surface membrane or the specific conductance G_m of the inner membranes could not be determined separately at each location. Model calculations and curve fitting show that the surface capacitance C_s had its largest effect on the impedance data recorded at the outer location and a small effect on the impedance data recorded from the inner location. Therefore, its value was usually determined by the curve fit to the outer data; C_s was held fixed during the curve fit to the inner data. The parameter G_m was best determined by the inner data. It was usually, therefore, held fixed to its inner value when the outer data was fit.

The radial variation of the intracellular resistivity R_i evident in Table I was disappointing, since the uniform theory used to interpret the impedance measurements assumed no variation. For that reason, a nonuniform theory was constructed in which the lens is divided into two regions (see Theory section and Appendix), a spherical nucleus surrounded by a cortex of

different properties. It would undoubtedly be preferable to construct a theory allowing a more continuous variation of properties, but neither the available morphometric data nor the mathematical skills of the present authors warrant such an effort.

The main body of measurements was made with the procedures and circuits described in Methods. The measurements were interpreted with the nonuniform theory to give estimates of the circuit parameters, particularly the effective intracellular resistivity. The magnitude and phase angle of the impedance were recorded at several locations of the voltage recording electrode, with the current electrode near the center of the lens (Fig. 5 and 6). The nonuniform theory was fit to a composite data set, consisting of data from all the electrode locations (see Methods), and the average properties of the lens were determined as the parameters of the theory necessary to make the best fit to the composite data set. The average parameters are shown in Table II and the fit to the composite data is shown in Fig. 7. Note that the effective intracellular resistivity of the outer region is called R_i and the ratio of the effective intracellular resistivity in the inner region to that in the outer region is called α. The misfits obvious in Fig. 7, and even more obvious in other data not shown, probably arise from local variation in the properties of the lens. We suspect that some of the variation is intrinsic to the lens and some is induced by the penetration of the microelectrode.

Fits were then made of the individual data sets taken at each electrode location, allowing only the intracellular resistivity in the outer region to vary, with all other parameters being held constant at their average values (determined from the previous fit to the composite data). Figs. 5 and 6 show representative fits at each location. Fig. 8 and Table III show the radial variation of the estimates of intracellular resistivity in the outer region. The variation of internal resistivity does not show systematic trends. The variation of R_i is a different expression of the misfits at different locations seen earlier in Fig. 7. If the curve fit program is allowed to use different values of R_i at different locations, it can better fit the data at different

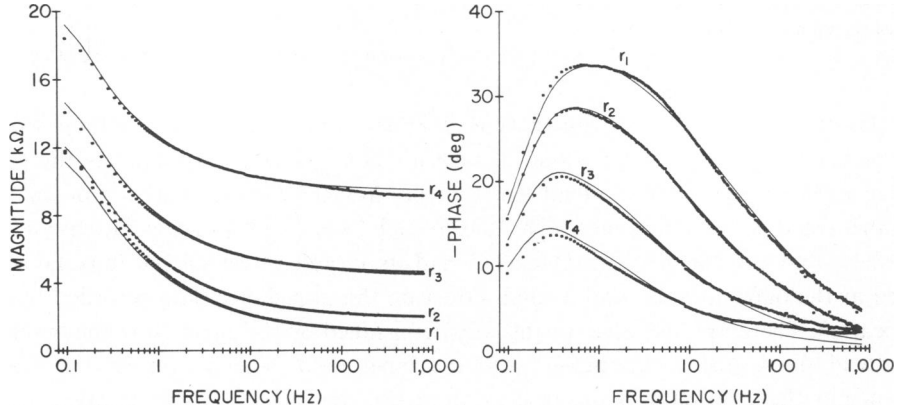

FIGURE 5 The magnitude, phase angle, and theoretical fit to the impedance of the lens. The points represent the magnitude and phase angle of the impedance of lens 2–10 measured at four positions of the voltage microelectrode, with the current microelectrode being close to the center of the preparation. The theoretical curves were determined as the best fit of the nonuniform model when only the effective internal resistivity was allowed to depend on electrode location. The other parameters were held at their average values as defined in the text. The misfit of theory and experiment (compared with, for example, Fig. 8) is probably the result of local variation of the properties of the lens.

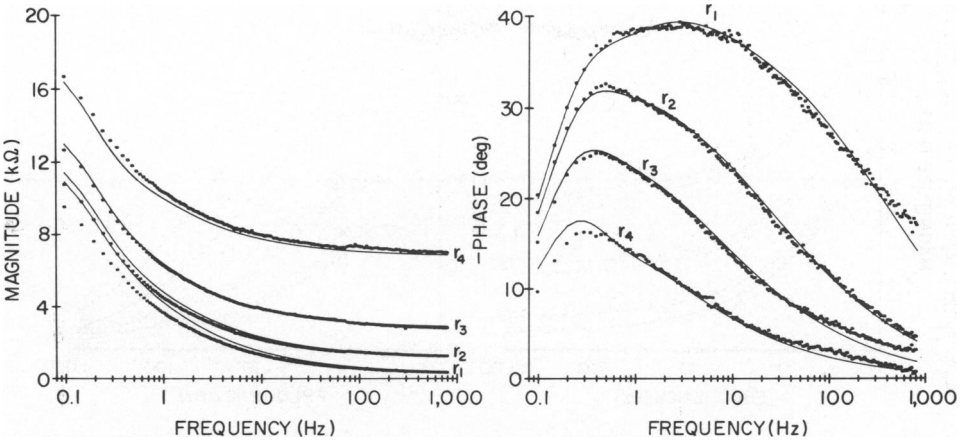

FIGURE 6 The magnitude, phase angle, and theoretical fit to the impedance of the lens. The points represent the magnitude and phase angle of the impedance of lens 2–8 measured at four positions of the voltage microelectrode, with the current microelectrode being close to the center of the preparation. The theoretical curves were determined as the best fit of the nonuniform model when only the effective internal resistivity was allowed to depend on electrode location. The other parameters were held at their average values as defined in the text. The misfit of theory and experiment (compared with, for example, Fig. 8) is probably the result of local variation of the properties of the lens.

locations than if it is constrained to use a single value of R_i, as in the earlier calculation of the average properties.

The general conclusion from the analysis is clear. A nonuniform theory allows a much better fit to experimental data than does a uniform theory. The nonuniform theory also has the virture of self-consistency: estimates of R_i made with the nonuniform theory are

TABLE II

AVERAGE PARAMETERS FROM CURVE FITS TO THE COMPOSITE DATA SET OF THE NONUNIFORM MODEL

Lens	Radius	V_m	G_s	C_s	C_m	G_m	R_i	α	R_e
	(mm)	*(mV)*	*(μS/cm²)*	*(μF/cm²)*	*(μF/cm²)*	*(μS/cm²)*	*(kΩ-cm)*		*(kΩ-cm)*
2–1	1.37	−71	322	3.4	1.02	0.54	3.6	2.3	60
2–2	1.38	−68	332	0.1	1.03	0.84	3.2	2.8	71
2–3	1.46	−79	235	6.5	1.03	0.31	3.0	2.5	69
2–4	1.47	−73	258	4.0	1.06	0.50	4.1	2.2	67
2–5	1.37	−71	378	5.3	1.33	1.18	4.8	2.6	118
2–6	1.34	−75	139	5.2	1.74	1.20	2.8	3.4	88
2–7	1.36	−68	256	3.3	1.03	1.00	4.4	2.5	73
2–8	1.33	−66	80	0.7	2.73	2.02	3.5	1.8	92
2–9	1.47	−70	343	3.4	0.96	0.41	3.7	2.2	52
2–10	1.35	−67	132	1.0	1.72	1.16	2.8	2.4	67
2–11	1.39	−70	288	4.5	0.89	1.25	3.7	2.2	51
					Summary				
Mean	1.39	−71	251	3.4	1.32	0.94	3.6	2.4	74
SEM	0.06	1	29	0.6	0.17	0.15	0.2	0.1	6

α is the ratio of the effective intracellular resistivity in the inner region to that in the outer region. R_i is the effective intracellular resistivity in the outer region.

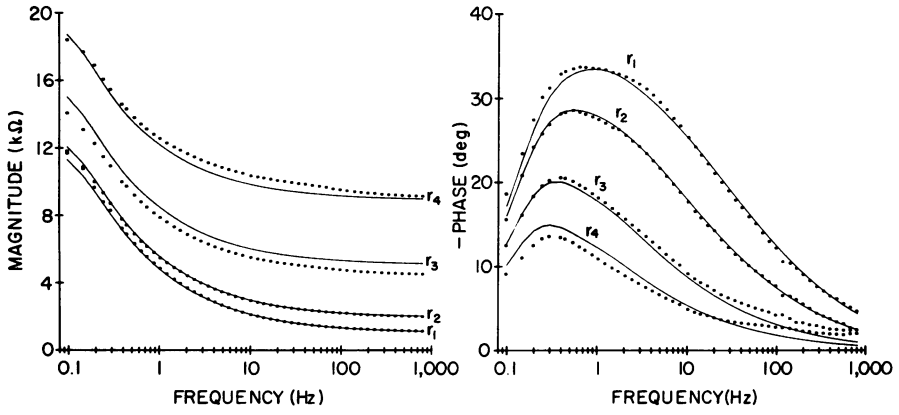

FIGURE 7 The magnitude, phase angle, and theoretical fit to the impedance of lens 2–10. The data are identical to Fig. 5. The theoretical curves determine the average circuit parameters. The nonuniform theory was fit to a composite data set consisting of points measured at each of the four radial locations (see text). The theoretical curves for each location are thus calculated with the same set of circuit parameters.

consistent with the behavior of R_i assumed in the derivation of the theory. Such consistency does not occur when the uniform theory is used.

It is much easier to record electrical properties once, at a single location with the voltage recording electrode close to the outside of the lens, than to record them many times at different locations. Indeed, previous impedance measurements from the lens have been made at just one location (Mathias et al., 1979). We fit data from a single location (Fig. 9) with the

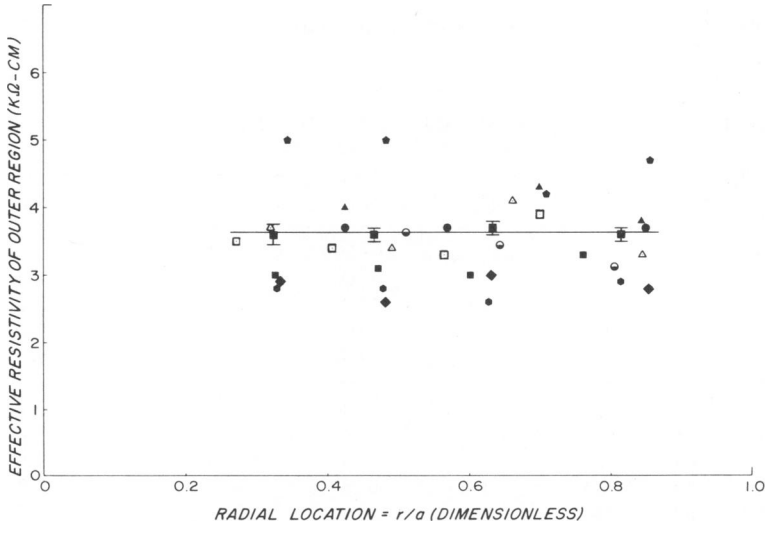

FIGURE 8 The variation of effective extracellular resistivity in the cortex with radial location. The figure is a plot of the data shown in Table III. Each symbol represents a different lens. The mean and standard error of the mean are shown for each location. The solid line is the mean of all measurements of R_i. If the nonuniform theory precisely described the data, there would be no systematic variation in the estimate of R_i.

TABLE III

RADIAL VARIATION OF EFFECTIVE INTERNAL RESISTIVITY OF THE NONUNIFORM MODEL

Lens						Mean
2–1	r*	1.10	0.90	0.70	—	
	R_i	3.1	4.1	3.6	—	3.6
2–2	r	1.05	0.83	0.65	0.45	
	R_i	3.3	3.0	3.1	3.0	3.1
2–4	r	1.23	1.02	0.62	—	
	R_i	3.8	4.3	4.0	—	4.0
2–5	r	1.17	0.97	0.66	0.47	
	R_i	4.7	4.2	5.0	5.0	4.7
2–6	r	1.09	0.84	0.64	0.44	
	R_i	2.9	2.6	2.8	2.8	2.8
2–7	r	1.12	0.82	0.66	0.46	
	R_i	4.4	4.5	4.0	4.3	4.3
2–8	r	0.93	0.75	0.54	0.36	
	R_i	3.9	3.3	3.4	3.5	3.5
2–9	r	1.24	0.97	0.72	0.47	
	R_i	3.3	4.1	3.4	3.7	3.6
2–10	r	1.15	0.85	0.65	0.45	
	R_i	2.8	3.0	2.6	2.9	2.8
2–11	r	1.18	0.79	0.59	—	
	R_i	3.7	3.7	3.7	—	3.7
			Summary			
Mean	R_i	3.6	3.7	3.6	3.6	3.6
SEM		0.2	0.2	0.2	0.3	0.2

The radius, resting potential, and other circuit parameters are shown in Table II. Experiment 2–3 was not successful enough to allow complete analysis.

*r in millimeters; R_i in kilohm-centimeters.

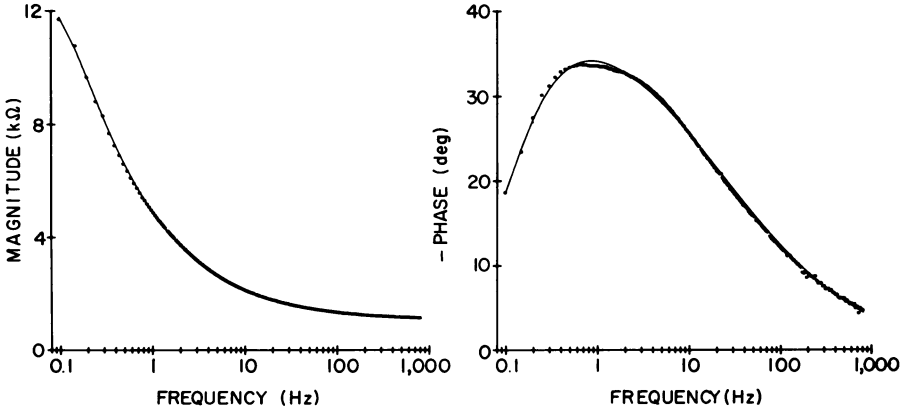

FIGURE 9 The magnitude, phase angle, and theoretical fit to impedance data of lens 2–8 taken from one electrode location. The electrode was at r_1 = 0.93 mm in a lens of radius a = 1.33 mm. The circuit parameters determined from the outermost location of the electrode are quite close to the average parameters determined from many locations (Table IV).

TABLE IV

PARAMETERS DETERMINED FROM THE OUTERMOST LOCATION OF THE VOLTAGE ELECTRODE USING THE NONUNIFORM MODEL

Lens	G_s	C_s	C_m	G_m	R_i	R_e
	($\mu S/cm^2$)	($\mu F/cm^2$)	($\mu F/cm^2$)	($\mu S/cm^2$)	(kΩ-cm)	(kΩ-cm)
2–1	359	3.4	0.96	0.50	2.9	47
2–4	301	4.0	0.87	0.64	3.4	48
2–5	377	5.0	0.74	1.05	4.6	61
2–6	171	6.2	1.14	0.76	2.8	59
2–7	339	4.3	0.88	0.90	3.9	52
2–8	104	2.6	1.31	1.28	4.2	52
2–9	390	4.0	0.94	0.38	3.1	43
2–10	243	0.2	1.25	0.73	2.3	38
2–11	323	4.7	0.77	0.90	3.5	42
			Summary			
Mean	290	3.8	0.99	0.79	3.4	49
SEM	33	0.6	0.07	0.09	0.3	3

The lens radius and the location of the electrode are given in Tables II and III. Experiments 2–2 and 2–3 were not successful enough to allow complete analysis.

nonuniform theory to see if systematic errors in the estimates of parameters resulted. Table IV shows the results of fits to the surface data of 9 of the 11 preparations illustrated in Tables II and III. In these fits α the ratio of the effective resistivity in the inner region to the effective resistivity in the outer region, was held fixed at the mean value 2.4 determined from measurements of radial variation (Table II). The parameters determined from one location are quite similar to the parameters determined at many locations. The approximate equality of parameters is gratifying, since it lessens the need for future measurements at many locations.

Note that fits of the nonuniform theory to data from one location (near the outer surface of the lens) determine all the electrical parameters, except the effective intracellular resistivity of the nuclear region αR_i. The reason for this is apparent from the equivalent circuit and discussion of the Theory section: the value of the intracellular resistivity in the nucleus is (electrically) too far from the outer surface, where the voltage electrode is located, to have much effect on the impedance. Therefore, the nuclear intracellular resistivity cannot be determined from measurements at the outer surface alone. This value can either be assumed from previous work, or can be measured by placing the voltage electrode in the nucleus of the lens.

DISCUSSION

Our results provide accurate measurements of the effective intracellular resistivity in both the nucleus and cortex of the lens. The improvements in circuitry and technique described here reduce the variance and duration of measurement, thus significantly improving the experimental data. These improvements should be useful for microelectrode recording in general since they can be directly applied to most experimental situations. The nonuniform theory derived here is self-consistent and provides a more realistic description of the lens than the earlier uniform theory.

A possible concern about the nonuniform theory is its treatment of the outer surface of the lens. The boundary condition for the nonuniform theory allows radial nonuniformity in the properties of the syncytia, but still assumes circumferentially uniform properties for the outer surface. The distribution of cuboidal epithelial cells is highly nonuniform, however, with the epithelia being confined to the anterior surface. The discrepancy between the actual structure of the surface of the lens and the assumed boundary condition is more troubling in theory than in practice: inclusion of circumferential variation of the boundary condition in the theory would not change the dominant term of the solution, the terms called $U_{i,e}^{(0)}$. The only effect would be in the second order terms $U_{i,e}^{(1)}$. The nonuniform distribution of epithelial cells has little effect because the bathing solution and gap junctions tend to short-circuit circumferential variation in potential. A quantitative evaluation of the effect of circumferential variation on the second order term is a complex problem, since the solution of mixed boundary value problems (i.e., problems with different properties on different regions of the boundary) are involved, and sometimes not possible in closed form. Qualitatively, one suspects that as long as the current electrode is in the center of the preparation, and as long as the potential is found experimentally to be symmetrical around the lens, the errors involved will be minimal. We conclude, then, that the surface parameters determined by our procedure are the averages of the properties of the anterior epithelial cells and a layer of both posterior and anterior lens fibers.

The effective intracellular resistivities reported here are called "effective" because they depend on the properties of the gap junctions between cells, as well as on the resistivity of the solution filling the lens fibers. The resistance of one gap junction, and the distribution and number of gap junctions, are important determinants of the effective intracellular resistivity. Indeed, one suspects that the nonuniformities and anisotropies in effective resistivity are for the most part caused by nonuniformities in the number and distribution of gap junctions.

Two nonuniformities are clear at this stage. The work reported here shows that the effective intracellular resistivity in the nuclear region of the lens is substantially larger than in the surrounding cortex. Comparision of our present results with earlier work (Eisenberg and Rae, 1976) reveals another kind of nonuniformity, an anisotropy in effective intracellular resistivity. The circumferential effective intracellular resistivity is 600 Ω-cm, while the radial effective intracellular resistivity is 3–4 kΩ-cm. Some of the difference in these figures is caused by the geometry of the preparation. Current can flow circumferentially entirely within lens fibers without crossing gap junctions. Furthermore, the flattened shape of lens fibers would produce anisotropy even if gap junctions were uniformly distributed. Nonetheless, it seems likely that the distribution of gap junctions is a significant cause of anisotropy. The anisotropy would be easily explained if there were few gap junctions connecting the large flat faces of lens fibers, and many gap junctions lining the angular edges of the fibers. Similarly, the presence of more gap junctions in the outer region than in the inner region would explain the radial variation of effective intracellular resisitivy reported here. Confirmation of these guesses requires morphological measurements of the distribution of gap junctions and a more precise analysis of current flow within the intracellular medium.

There may well be other nonuniformities in lens properties which our techniques have not detected. For example, it is clear from model calculations that radial variation in the effective extracellular resistivity would not be measured by our method. Equivalently, radial variation in the amount of membrane area per volume of tissue would be difficult to detect. Physically,

it is clear that either kind of variation would have substantial effects on the distribution of extracellular potential. But our measurements, confined as they have been to the intracellular domain, are shielded from the extracellular potential by the inner membranes (Eisenberg et al., 1979) and therefore smooth over the consequences of the distribution of extracellular potential.

This smoothing reduces the spatial resolution of our measurements: neither local nor radial variation of the effective extracellular resistivity can be detected by our measurements. However, the smoothing is also an advantage, since the random variations in the structure of the extracellular space are likely to be larger than in the intracellular space, and the effects of the electrode track through the tissue are also likely to more important in the extracellular space. Thus, random variations in the extracellular potential might be large enough to obscure systematic radial variations if they were measured directly; for example, by direct measurement of extracellular potential. Our measurement of intracellular potential, then, has the advantage of being insensitive to some of the more uninteresting variations of extracellular properties, local variation, and electrode damage, but it has the disadvantage of insensitivity to systematic variation of extracellular properties.

Our techniques seem sensitive enough to measure random variations in intracellular properties. The misfits of the theory to the composite data set (consisting of data from many locations) and, equivalently, the variation of R_i, seen in Fig. 8, are such examples.

Despite these difficulties, it seems clear that the present experiments provide reasonably accurate estimates of the resting electrical properties of the different membranes of the lens. It will be of interest to determine the ionic basis of these properties and to determine the structural and ionic source of the nonlinear properties reported by some workers (Patmore and Duncan, 1979).

It is a pleasure to thank Mr. T. Tinor for his excellent programming and patient execution of multiple versions of the theoretical model.

This work was supported by National Institutes of Health grants EY 03095, EY 03282, and HL 20230.

Received for publication 2 July 1980 and in revised form 15 October 1980.

APPENDIX

The Appendix provides an outline of the solution of the differential equations for a nonuniform spherical syncytium as defined in the Theory section. As the derivation follows the steps of Eisenberg et al. (1979) fairly closely, many details are omitted. We adopt the nomenclature of that paper with a few exceptions noted immediately below (note the new definition of R_i and of the normalized potentials). All dimensionless variables are boldface.

The dimensional differential equations are normalized as described in Eisenberg et al. (1979) with

$$\epsilon = \frac{R_i}{R_i + R_e}; \qquad \kappa = \frac{\gamma Y_s}{(S_m/V_T)Y_m};$$

$$\gamma^2 = (R_i + R_e)(S_m/V_t)Y_m; \qquad \mathbf{U}_{i,e} = \frac{U_{i,e}}{i_L \alpha \gamma (R_i + R_e)}, \quad \text{(A-1)}$$

where R_i is the effective intracellular resistivity in the outer shell (the cortex), defined by $b \leq r \leq a$. The substitution of an expansion for $U_{i,e}$ in powers of ϵ into the dimensionless version of the differential

equations and boundary conditions gives a series of problems for different orders of the potential in the intracellular and extracellular media. The solutions to the first order problems are

$$\mathbf{U}_i^{(0)}(\mathbf{r}) \equiv \mathbf{C}_0 = \frac{1}{4\pi\alpha(\gamma a)^2[\kappa + \coth(\gamma a) - 1/\gamma a]} \tag{A-2}$$

$$\mathbf{U}_e^{(0)}(\mathbf{r}) = \mathbf{C}_0\left[1 - \frac{\gamma a \sinh \mathbf{r}}{\mathbf{r} \sinh \gamma a}\right]. \tag{A-3}$$

The problems for the order one potentials will take most of our attention. For the intracellular potential we can write the problems for each region, remembering that the current source is placed in the center of the tissue.

$$\nabla^2\mathbf{U}_i^{(1-)} = \alpha[\mathbf{C}_0 - \mathbf{U}_e^{(0)}(\mathbf{r})] - \frac{\delta(\mathbf{r})}{4\pi\mathbf{r}^2} \tag{A-4}$$

$$\nabla^2\mathbf{U}_i^{(1+)} = \mathbf{C}_0 - \mathbf{U}_e^{(0)}(\mathbf{r}); \qquad \frac{d\mathbf{U}_i^{(1^*)}(\gamma a)}{d\mathbf{r}} = -\kappa\mathbf{C}_0. \tag{A-5}$$

We define a Green's function $\mathbf{G}(\mathbf{r})$ for the Dirichlet problem for the intracellular space.

$$\nabla^2\mathbf{G}(\mathbf{r}) = \frac{-1}{\alpha}\delta(\mathbf{r}); \qquad \mathbf{G}(\gamma a) = 0 \tag{A-6}$$

which has the solution

$$\mathbf{G}(\mathbf{r}) = \frac{1}{4\pi\alpha\gamma a}\left(\frac{\gamma a}{\mathbf{r}} - 1\right). \tag{A-7}$$

Using the matching condition at $r = \gamma b$, we can write the solution of these problems in terms of $\mathbf{G}(\mathbf{r})$ and a yet to be determined "constant" $\boldsymbol{B}$:

$$\mathbf{U}_i^{(1-)}(\mathbf{r}) = -\alpha[\mathbf{U}_e^{(0)}(\mathbf{r}) + \mathbf{U}_e^{(0)}(0)] + \alpha\mathbf{G}(\mathbf{r}) + (1 - \alpha)(\mathbf{G}(\gamma b) - \mathbf{U}_e^{(0)}(\gamma b) - \mathbf{U}_e^{(0)}(0)) + \mathbf{B} \tag{A-8}$$

$$\mathbf{U}_i^{(1^*)}(\mathbf{r}) = -(\mathbf{U}_e^{(0)}(\mathbf{r}) + \mathbf{U}_e^{(0)}(0)) + \mathbf{G}(\mathbf{r}) + \mathbf{B}. \tag{A-9}$$

The form assumed for the solution reduces the algebraic complexity of the problem since components of the solution individually satisfy the differential equation and one of the boundary conditions.

The order one extracellular problem must be written in two regions, because the driving function (i.e., the right-hand side of the differential equations) has a different form in each of the regions.

$$\nabla^2\mathbf{U}_e^{(1-)} - \mathbf{U}_e^{(1-)} = -\mathbf{U}_i^{(1-)} + \mathbf{C}_0 - \mathbf{U}_e^{(0)}(\mathbf{r}) \tag{A-10}$$

$$\nabla^2\mathbf{U}_e^{(1+)} - \mathbf{U}_e^{(1+)} = -\mathbf{U}_i^{(1+)} + \mathbf{C}_0 - \mathbf{U}_e^{(0)}(\mathbf{r}); \qquad \mathbf{U}_e^{(1+)}(\gamma a) = 0. \tag{A-11}$$

We define an extracellular Green's function $\mathbf{W}(\mathbf{r})$ for the extracellular Dirichlet problem

$$\nabla^2\mathbf{W} - \mathbf{W} = -\frac{1}{\alpha}\delta(\mathbf{r}); \qquad \mathbf{W}(\gamma a) = 0 \tag{A-12}$$

which has the solution

$$\mathbf{W}(\mathbf{r}) = \frac{\cosh \gamma a}{4\pi\alpha\gamma a}\left(\frac{\gamma a}{\mathbf{r}}\frac{\cosh \mathbf{r}}{\cosh \gamma a} - \frac{\gamma a}{\mathbf{r}}\frac{\sinh \mathbf{r}}{\sinh \gamma a}\right). \tag{A-13}$$

Now, we can write the solution of the extracellular outer problem in terms of the Green's function and the yet to be determined parameters **B** and **C**. **B** and **C** are constants in the sense that they are independent of r; they are, however, functions of a multitude of other variables. Note that when $C = 0$ we recover the solution of Eisenberg et al. (1979). The form of the solution is again chosen for convenience in applying boundary conditions

$$\mathbf{U}_e^{(1+)}(\mathbf{r}) = -\mathbf{U}_e^{(0)}(\mathbf{r})\left[1 - \frac{\mathbf{B} - \mathbf{U}_e^{(0)}}{\mathbf{C}_0}\right] + \mathbf{G}(\mathbf{r}) - \mathbf{W}(\mathbf{r}) + \mathbf{C}\mathbf{W}(\mathbf{r}). \tag{A-14}$$

Next we apply the integral constraint for the order one problem.

$$\kappa[\mathbf{C}_0 - \mathbf{U}_i^{(1+)}(\gamma a)] + \frac{d\mathbf{U}_e^{(1+)}(\gamma a)}{d\mathbf{r}} = -\mathbf{G}'(\gamma a) \equiv \frac{d\mathbf{G}(\gamma a)}{d\mathbf{r}} = -\frac{1}{4\pi\alpha\gamma^2 a^2}. \tag{A-15}$$

The integral constraint (Eq. A-15) and integral constraint for the order zero problem gives a relation between **B** and **C**. Note that prime means differentiation with respect to the dimensionless variable **r**.

$$\mathbf{B} = -\mathbf{C}_0 \frac{\mathbf{W}'(\gamma a)}{\mathbf{G}'(\gamma a)} \mathbf{C} = -\mathbf{C}[\mathbf{C}_0 - \mathbf{U}_e^{(0)}] \tag{A-16}$$

$$\mathbf{W}'(\mathbf{r}) = \frac{\cosh \gamma a}{\alpha 4\pi \mathbf{r}}\left[\frac{\sinh \mathbf{r}}{\cosh \gamma a} - \frac{\cosh \mathbf{r}}{\mathbf{r} \cosh \gamma a} + \frac{\sinh \mathbf{r}}{\mathbf{r} \sinh \gamma a} - \frac{\cosh \mathbf{r}}{\sinh \gamma a}\right]. \tag{A-17}$$

To evaluate the constant **C**, we must solve the differential equation for $\mathbf{U}_e^{(1-)}(r)$ and introduce a new "constant" **D**.

$$\mathbf{U}_e^{(1-)}(\mathbf{r}) = \mathbf{U}_e^{(1+)}(\mathbf{r}) - \mathbf{C}\mathbf{W}(\mathbf{r}) + \mathbf{D}\frac{\gamma b \sinh \mathbf{r}}{\mathbf{r} \sinh \gamma b} + (1 - \alpha)[\mathbf{U}_e^{(0)}(\mathbf{r}) - \mathbf{U}_e^{(0)}(\gamma b) - \mathbf{G}(\mathbf{r}) + \mathbf{G}(\gamma b) + \mathbf{\Pi}(\mathbf{r})] \tag{A-18}$$

where

$$\mathbf{\Pi}(\mathbf{r}) \equiv \mathbf{W}(\mathbf{r}) + \mathbf{C}_0 \frac{\gamma a \cosh \mathbf{r}}{2 \sinh \gamma a} - \frac{\gamma b \sinh \mathbf{r}}{\mathbf{r} \sinh \gamma b}\left[\mathbf{W}(\gamma b) + \mathbf{C}_0 \frac{\gamma a \cosh \gamma b}{2 \sinh \gamma a}\right]. \tag{A-19}$$

We apply a continuity condition $\mathbf{U}_e^{(1-)}(\gamma b) = \mathbf{U}_e^{(1+)}(\gamma b)$ to write **D** in terms of **C**:

$$\mathbf{D} = \mathbf{C}\,\mathbf{W}(\gamma b). \tag{A-19}$$

Application of the matching condition for the spatial derivative of the extracellular potential at $\mathbf{r} = \gamma b$ gives the explicit expression for **C** written in Eq. 15 of the text.

REFERENCES

EISENBERG, R. S., and P. W. GAGE 1969. Ionic conductances of the surface and transverse tubular membranes of frog sartorius fibers. *J. Gen. Physiol.* **53**:279–297.

EISENBERG, R. S., and R. T. MATHIAS 1980. Structural analysis of electrical properties. *Crit. Rev. Bioeng.* **4**:203–232.

EISENBERG, R. S., and J. L. RAE. 1976. Current-voltage relationships in the crystalline lens. *J. Physiol. (Lond.).* **262**:285–300.

EISENBERG, R. S., V. BARCILON, and R. T. MATHIAS 1979. Electrical properties of spherical syncytia. *Biophys. J.* **25**:151–180.

FALK, G, and P. FATT. 1964. Linear electrical properties of striated muscle fibers observed with intracellular electrodes. *Proc. R. Soc. Lond. B. Biol. Sci.* **160**:69–123.

HOGAN, M. J., J. A. ALVARADO, and J. E. WEDDELL. 1971. Histology of the Human Eye. W. B. Saunders Company, Philadelphia. 638–677.

MATHIAS, R. T., J. L. RAE, and R. S. EISENBERG. 1979. Electrical properties of structural components of the crystalline lens. *Biophys. J.* **25**:181–201.

PATMORE, L., and G. DUNCAN. 1979. A TEA-sensitive component in the conductance of a non-excitable tissue (the amphibian lens). *Exp. Eye Res.* **28**:349–352.

RAE, J. 1979. The electrophysiology of the crystalline lens. *Curr. Top. Eye Res.* **1**:37–90.

SMITH, John I. 1971. Modern Operational Circuit Design. John Wiley & Sons, Inc., New York.

SUZUKI, K., V. ROHLICEK, and E. FROMTER. 1978. A quasi-totally shielded, low-capacitance glass-microelectrode with suitable amplifiers for high-frequency intracellular potential and impedance measurements. *Pflugers Arch. Eur. J. Physiol.* **378**:141–148.

TANAKA, M., P. RUSSELL, S. SMITH, S. UGA, T. KUWABARA, and J. KINOSHITA. 1980. Membrane alterations during cataract development in the Nakano mouse lens. *Invest. Opthamol. Visual Sci.* **19**:619–629.

VALDIOSERA, R., C. CLAUSEN, and R. S. EISENBERG. 1974. Measurement of the impedance of frog skeletal muscle fibers. *Biophys. J.* **14**:295–315.